

The displacement of the thermally grown oxide in thermal barrier systems upon temperature cycling

A.M. Karlsson^{a,*}, J.W. Hutchinson^b, A.G. Evans^c

^a Department of Mechanical Engineering, University of Delaware, Newark, DE 19716, USA

^b Division of Engineering and Applied Science, Harvard University, Cambridge, MA 02138, USA

^c Materials Department, University of California, Santa Barbara, Santa Barbara, CA 93106, USA

Received 4 June 2002; received in revised form 28 October 2002

Abstract

Models that characterize the displacement instability of the thermally grown oxide (TGO) found in some thermal barrier systems are reviewed, consolidated and extended. It is demonstrated that the simulations are only consistent with the observations whenever the bond coat and TGO both undergo plastic deformation. The TGO yields at the peak temperature, during growth, while the bond coat yields on thermal cycling. The trends oppose. Namely, the TGO displacement is diminished by increasing the high temperature strength of the bond coat, but is increased upon increasing the TGO strength. The model rationalizes certain experimental trends, particularly the decrease in durability as the hot time per cycle decreases. Interactions between the instability and cracks in the thermal barrier layer are discussed.

© 2002 Elsevier Science B.V. All rights reserved.

Keywords: Analytical model; Elastic–plastic material; Finite elements; Thermal barrier coatings; Thermal cycling; Oxidation

1. Introduction

Thermal barrier systems used in gas turbines have been comprehensively described in recent overview articles [1–7]. These assessments have elaborated the benefits and have confronted the need for a system level approach to design and durability. The emphasis has been on failure modes governed by the thermally grown oxide (TGO) [8–22], predominantly α -Al₂O₃, that forms between the thermal barrier coating (TBC) and the bond coat (Fig. 1). This thin layer develops large residual compressive stress because of growth and thermal expansion misfit, causing the layer to be unstable against out-of-plane displacements (Fig. 2). The occurrence of the instability is largely dictated by the mechanical characteristics of the bond coat. Non-planarity and imperfections in the TGO are also important (Fig. 3) [12–16,18–22]. Bond coats most susceptible to this instability are those with composi-

tions in the β -phase field, because of the relatively inferior high temperature strength of this phase. The most widely documented example occurs in the bond coat referred to as Pt–aluminide, illustrated with the Ni–Al–Pt ternary phase diagram (Fig. 4) [23]. An important goal is to understand how the instability is affected by the properties of the constituent materials, in order to design a system that suppresses the mechanism, without introducing a more deleterious failure mode.

The attempts made to understand the parameters that affect this instability are encapsulated in a series of papers that sequentially introduced the mechanistic elements required for a comprehensive model [12,14,19–21]. Unearthing the role of each constituent property has been challenging because of the strong coupling between the multiple contributions to the strains embodied in the mechanism. There are two objectives of this paper: (i) to describe these strains and discuss their mechanistic basis and (ii) to demonstrate how they interact, thereby establishing the separate roles of the constituent properties.

An important step has been the origination of a spherically symmetric model that, while geometrically

* Corresponding author

E-mail address: karlsson@me.udel.edu (A.M. Karlsson).

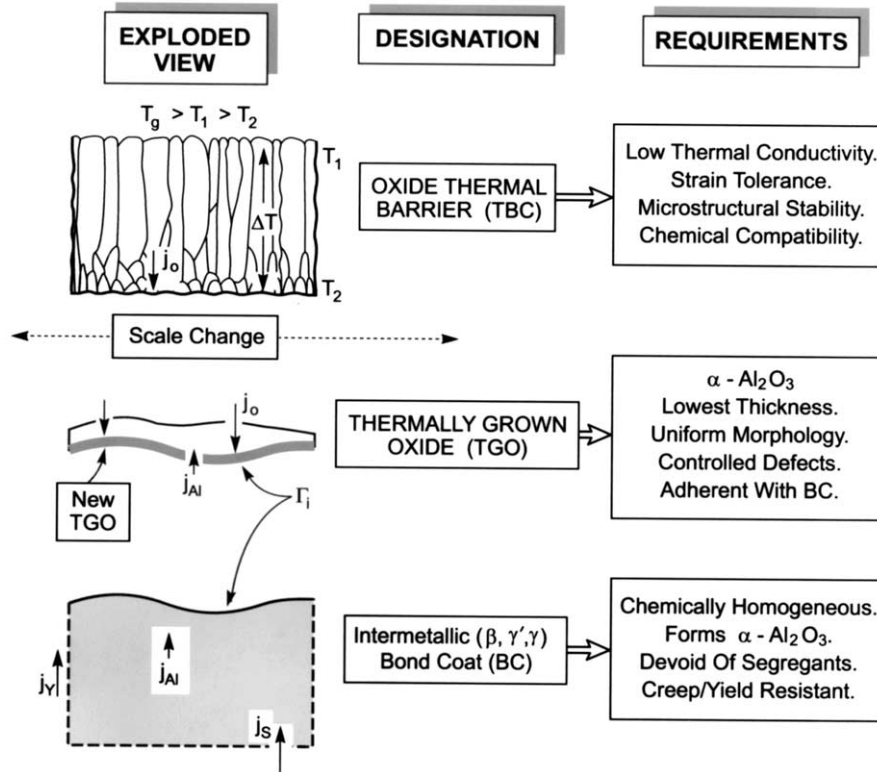


Fig. 1. An exploded view of a thermal barrier system that identifies the function of each layer.

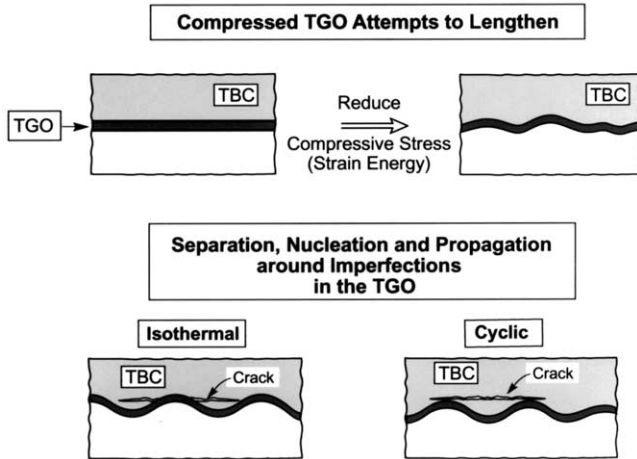


Fig. 2. A schematic of the out of plane displacement of the thin layer of TGO that relieves the large residual compression.

simplified, appears to correctly incorporate some of the physical effects [21] (Fig. 5). This model has close analogies with that used, successfully, to represent the indentation of a half space [24–26]. The basic idea is depicted on Fig. 5. In the vicinity of an imperfection in the TGO, the stresses induced by thermal contraction and growth exert a pressure on the bond coat similar to that caused by an indenting sphere. This causes yielding upon thermal cycling that accommodates the growth strains in the TGO, enabling the TGO to displace on a

cycle-by-cycle basis. The attribute of the model is that it allows multiple calculations that probe the separate roles of each of the material and geometric parameters.

Several other important effects are incompatible with the sphere model. One relates to the role of the TBC and the other to the strain misfit between the bond coat and the substrate (caused by thermal expansion and phase transformations). To address these issues, a full geometric model is required encompassing a substrate, a bond coat, a TGO and a TBC with a geometric imperfection in the TGO (Fig. 5A) [12,14,19,20].

2. The strain components

The strains generated by the TGO are basic to the instability: one component is caused by thermal expansion misfit and the other by TGO growth. Generally, these can be superposed as a net transformation strain per cycle, $\Delta\epsilon_T$. To provide perspective, each strain component is discussed separately.

2.1. Strain due to thermal misfit

The most straightforward to comprehend is that caused by thermal contraction misfit with the substrate. The consequences can be readily modeled by treating the TGO as elastic and the bond coat as elastic/plastic. Results applicable to thermal cycling exist for various

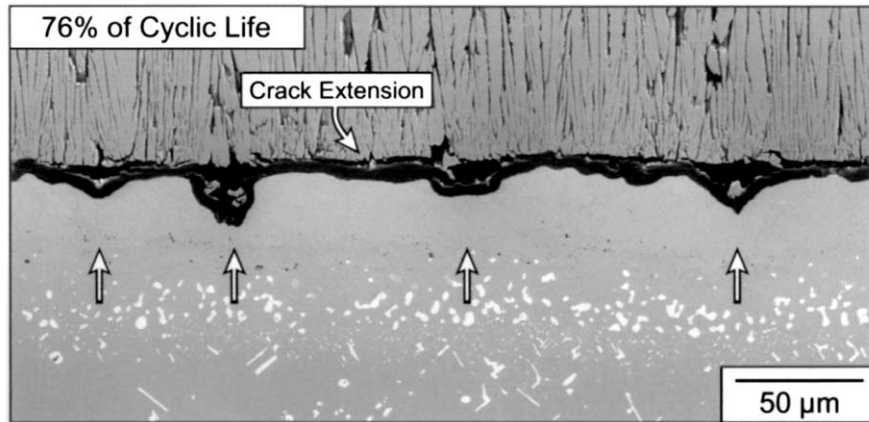


Fig. 3. Scanning electron microscope image showing the cracks that form in the above an imperfection that experiences TGO instability (courtesy Mumm).

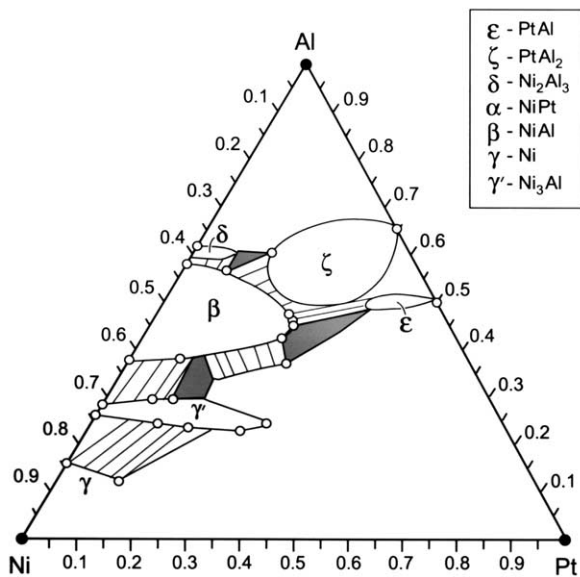


Fig. 4. The ternary phase diagram at 1100 °C for the Ni/Al/Pt system showing the β and γ' phases of interest.

non-planar surfaces [6,27]. A stationary strain loop develops after the first few cycles. In principle, the cyclic plastic strains could cause fatigue cracks in the bond coat, but in practice, this does not appear as a failure mode.

2.2. Strain due to TGO formation

The strains attributed to growth of the TGO exhibit more nuances. Conceptually, the process occurs as sketched on Fig. 6. An element of the bond coat (with ill-defined thickness) changes composition with a net diminution of Al. This Al reacts with ingressing O to form Al_2O_3 with an associated increase in volume. This process could happen in accordance with many different

scenarios. Determination of the scenario chosen by systems of practical interest requires input from experimental observations of the TGO. Three such observations and assessments are deemed critical:

(a) The columnar grain structure beneath an equiaxed initial layer (Fig. 7) indicates that new TGO forms primarily on the interface with the bond coat. This is believed to happen, because the diffusivity of oxygen along the TGO grain boundaries exceeds that for Al [28–32].

(b) The interface between the TGO and the bond coat is incoherent, discounting coherency strains. Accordingly, on a planar segment, the volume increase due to interface growth (thickening) is accommodated by an upward, rigid body displacement of the TGO, obviating the development of a stress. On curved segments the displacements cannot be accommodated by rigid body displacements and stresses are created with magnitude related to the ratio of new TGO volume to the consumed bond coat volume, taken to be m [33]. When the TGO and bond coat are both elastic, with the same modulus, the stresses within the TGO, thickness h , formed on a concave surface, radius R , are [33]:

$$\sigma_{rr} = -\frac{2E(m-1)h}{3(1-\nu)mR}$$

$$\sigma_{\theta\theta} = \sigma_{\theta\theta}^i + \frac{E(m-1)}{3(1-\nu)m} \left[\frac{r}{R} - \left(1 - \frac{h}{R} \right) \right] \quad (1)$$

where r is the distance from the center of curvature (Fig. 5B). The hoop stress $\sigma_{\theta\theta}^i$ at the growth interface is unspecified. It may be positive or negative. In practice, these stresses are relaxed by yielding of the bond coat and the TGO. They are also changed by TGO elongation.

(c) Some of the new TGO resides on the internal grain boundaries causing it to elongate when the constraint

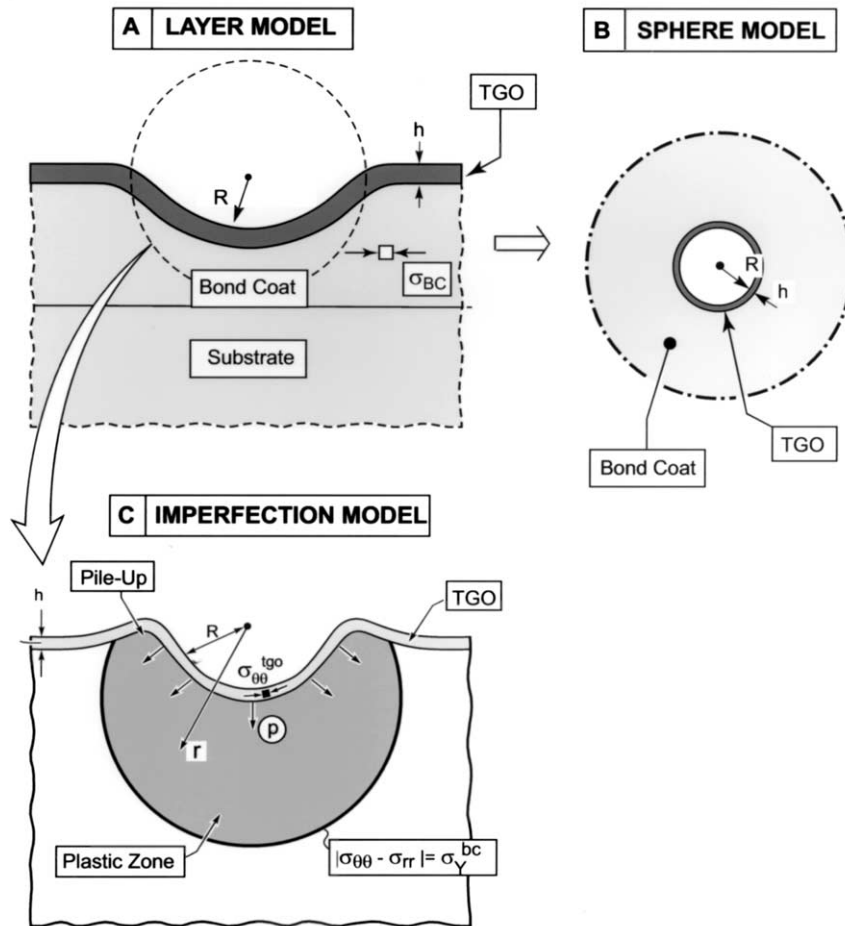


Fig. 5. The system interpreted as a layered model, a hemispherical imperfection and a spherical shell model. Geometrical aspects of deformations that occur around an imperfection motivated by TGO growth and thermal cycling.

from the bond coat is relaxed. The most direct evidence emerges from experiments on thin foils, which elongate upon isothermal oxidation [34,35]. A similar elongation of the TGO occurs, locally, around imperfections (Fig. 3). The elongation strain causes planar segments to develop in-plane compressive growth stress. This TGO growth mode is essential to instability propagation [14,35]. The responsible mechanism appears to be related to the existence of preferential sites for Al_2O_3 formation on the internal grain boundaries [36].

The growth strain in the TGO induces compressive growth stresses. The stress builds up as the thickness of the new Al_2O_3 on the grain boundaries increases. When this stress attains the plastic flow or creep strength (the relevant mechanisms are depicted on Fig. 8) [37], the internally-formed Al_2O_3 is redistributed by thickening of the TGO layer (consistent with volume conservation, via the plastic Poisson ratio). At the simplest level, the elongations and the stresses can be understood in terms of the two bar model on Fig. 9, wherein the strain

causing elongation is that induced by TGO formation on the internal grain boundaries.

2.3. Strain in the bond coat

The bond coat responds in a manner dictated by its flow strength. This strength is believed to have strong temperature and rate sensitivity (Fig. 10). However, data for actual bond coat alloys are sparse. Results for a Pt–aluminide system are summarized on Fig. 10 [38]. They can be idealized as high temperature strength, $(\sigma_Y^{bc})_{\min}$ above T_2 , between 5 and 50 MPa, with a rapid rise at lower temperatures. The response of interest is that above T_2 . At lower temperatures, the bond coat remains elastic: unless it is subject to a martensite transformation, which results in a volumetric strain upon cooling (Fig. 11) [39]. For practical purposes, instability propagation analysis can be confined to a cyclic range between T_2 and the temperature maximum,

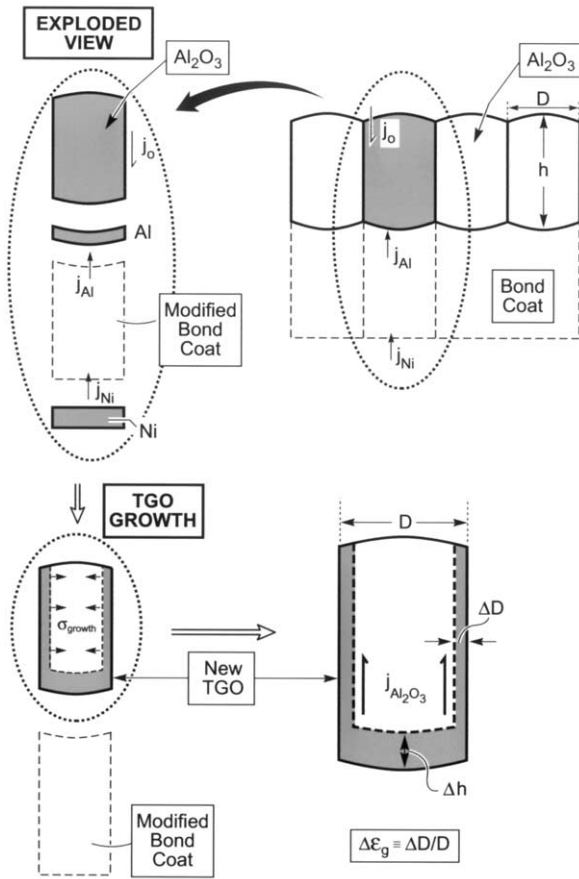


Fig. 6. Exploded view of the oxidation process indicating the sites for new oxide formation and the associated growth stresses. The oxide at the interface is accommodated by a rigid body displacement with no requirement for growth stress. The new oxide that forms on the internal grain boundaries must induce a stress.

with $\Delta T \equiv T_{\max} - T_2$, subject to bond coat yield strength, $(\sigma_Y^{bc})_{\min}$.

3. The sphere model

3.1. Analogous phenomena

The TGO can be envisaged as a shell under compression situated on a non-planar surface (Fig. 5A). In the vicinity of impressions, the TGO is in compression, because of growth and thermal expansion misfit. It imposes a normal pressure, p , on the bond coat (Fig. 5C) with magnitude that scales with the ratio of the TGO thickness, h , to the radius of curvature of the impression, R (therefore zero on flat sections). This pressure induces radial compression and tangential tension in the surrounding bond coat, and may exceed its yield strength. The consequent plastic zone has size and shape similar to that associated with the indentation of a half space by a rigid sphere [24–26,40,41]. The plastic strains are also similar. They are predominantly

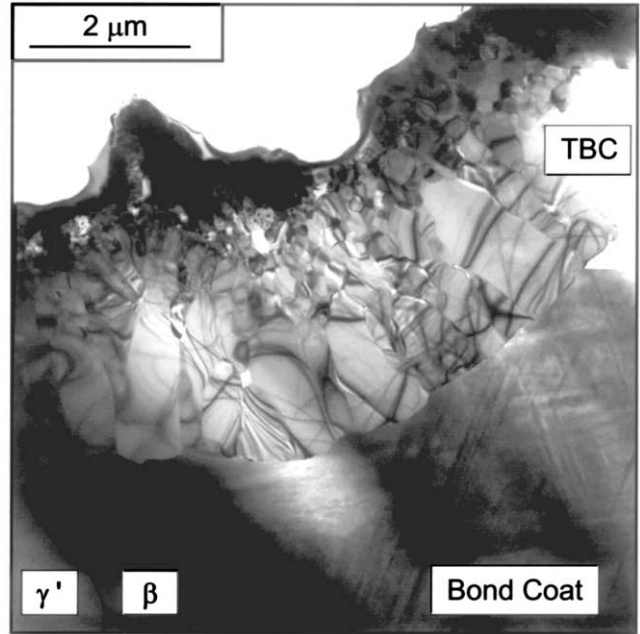


Fig. 7. Transmission electron microscope image of the TGO showing the columnar grain structure (courtesy Darzens).

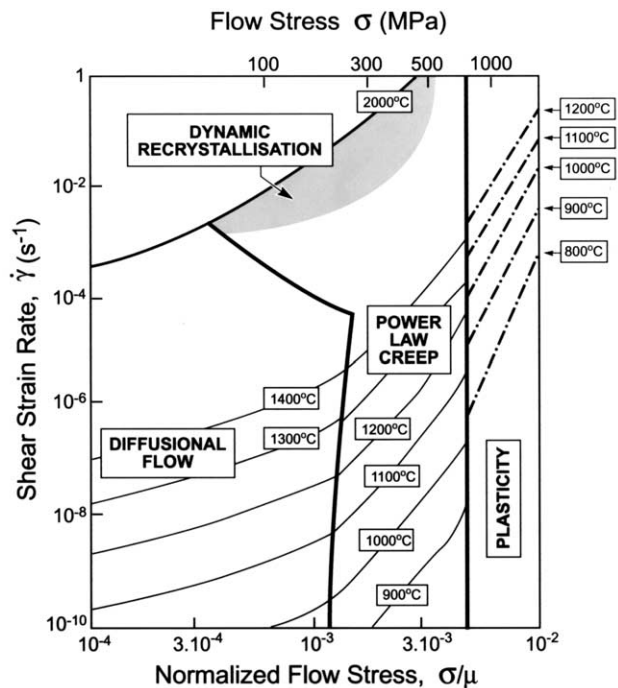


Fig. 8. Deformation mechanism map for α -Al₂O₃ with a grain size of 10 μ m. At 1 μ m the boundary between plasticity and power law creep is unchanged. The boundary between diffusion and power law creep moves to the right.

radial, except near the surface, where tangential strains induce pile up. Most aspects of the indentation response can be captured by adapting the solution for an expanding spherical cavity [24]. This model duplicates

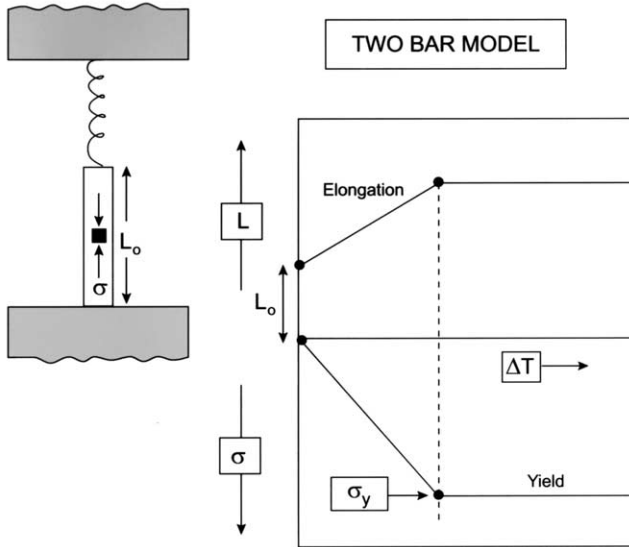


Fig. 9. A two bar model in which the solid plate is envisaged as the TGO and the spring as the bond coat. As elongation strain is introduced into the TGO, the stress builds up until it reaches its yield strength. Thereafter, despite the continuing addition of matter, since the stress must remain the same, the spring cannot contract further and the TGO remains at the same length. The extra matter is redistributed by thickening of the plate.

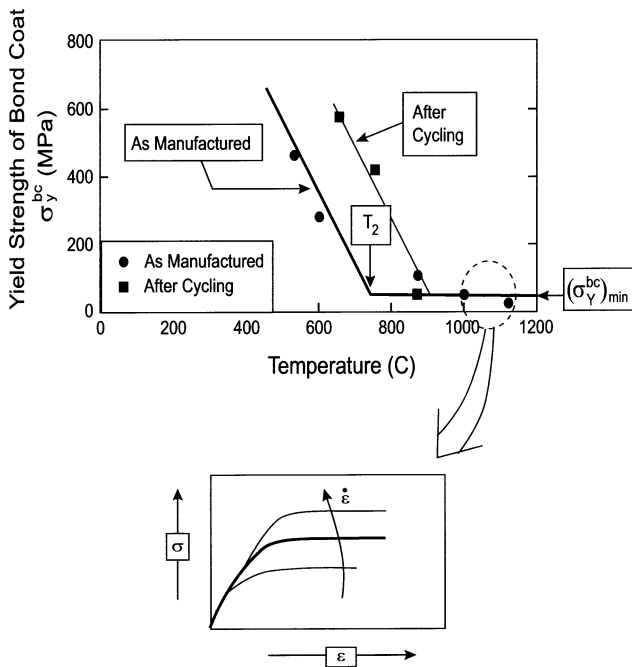


Fig. 10. Yield strength of a Pt–aluminide bond coat as a function of temperature [38]. The inset shows the stress/strain response at high temperature as a function of strain rate.

the radial displacements, the plastic zone and the stress state. Determining the pile up requires the introduction of the free surface. This analog is the inspiration for the Sphere Model (Fig. 5B) [21].

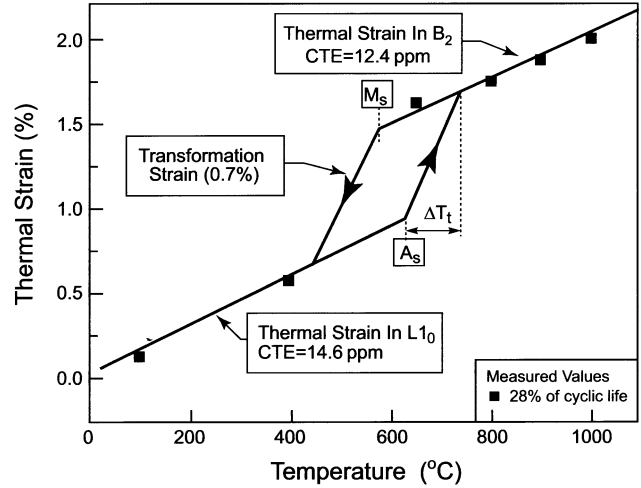


Fig. 11. The expansion and contraction of a Pt–aluminide in the β -phase caused by thermal expansion and martensite transformation [39].

3.2. Synopsis

A spherical TGO shell is attached to an infinite bond coat, taken to be elastically incompressible with Young’s modulus, E_{bc} , and yield strength, σ_Y^{bc} . Except at the highest temperature in the history, the TGO undergoes only elastic deformations governed by its Young’s modulus, E_{tgo} , and Poisson’s ratio, ν_{tgo} . At the peak temperature, T_{max} , the TGO is elastic/perfectly plastic with strength, σ_Y^{tgo} , at the strain-rates relevant to thermal cycling. The TGO exerts a pressure, p , on the bond coat and a circumferential stress, σ_{tgo} , is induced. The consequence is a radial displacement, u . There appear to be two primary domains: one operative when the TGO is thin (small h/R), the other when the TGO has finite thickness and the bond coat is soft. The basic trends are summarized on Figs. 12 and 13.

Each cycle begins (position 0 on Fig. 12) at the peak temperature, T_{max} , with a compressive stress in the TGO established by previous thermal cycles. For most practical scenarios, this stress is below the TGO strength. It is designated, $\sigma_{tgo}^{(0)}$ (Fig. 12a). During the first stage in the new cycle (0→3), a growth strain is imposed with thickening and elongation components. The relatively soft bond coats of greatest interest reach yield during the addition of the growth strain (at position 1), enhancing the radial displacement rate (Fig. 12b). Simultaneously, the elongation increases the TGO compression until it also yields (position 2). Once plastic deformation initiates in the TGO, the additional growth causes thickening with no further elongation. On cooling, starting at position 3, the stress in the bond coat increases and attains its yield strength at position 4. The consequent plastic strains between positions 4 and 5 accommodate the growth strain in the TGO. This is the step that enables the permanent displacement, Δu_{cycle}

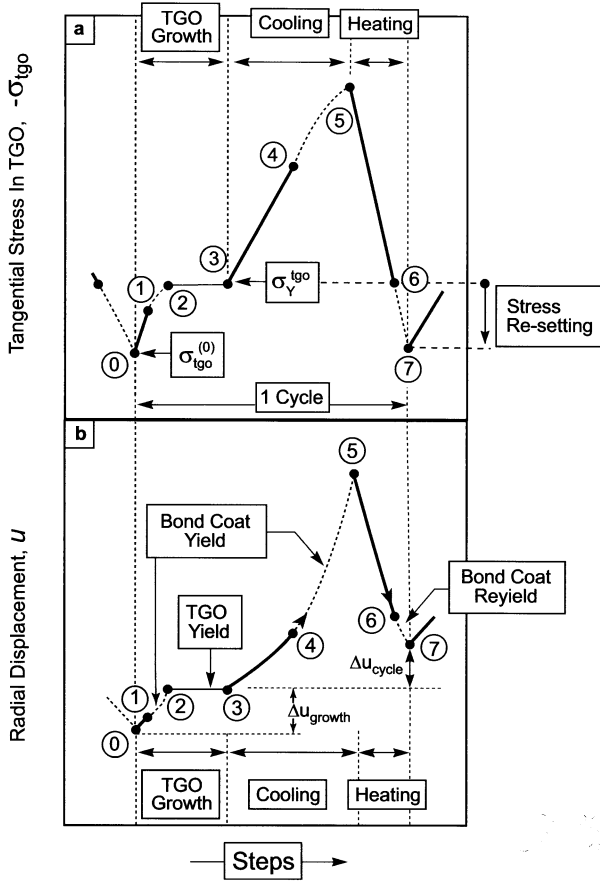


Fig. 12. The cyclic response of the TGO/bond coat system for one thermal cycle demonstrates how the (a) tangential compressive stress and (b) radial displacement evolve.

(Fig. 12b). That is, even though the transformation strain is introduced during the growth step, the displacements are manifest on cooling, through plastic straining of the bond coat. The reheating is elasticity dominated, such that, at the end of the reheat step (position 7), the stress in the TGO returns to that at the start of the cycle, $\sigma_{tgo}^{(0)}$, ‘resetting’ the stress (Fig. 12a), and allowing the process to repeat.

Isothermal and cyclic responses are differentiated, provided that the TGO reaches yield during the growth step [21]. Isothermally, the TGO yields and the stress remains at yield, such that all of the growth strain results in thickening without elongation, in accordance with the two bar model (Fig. 9). Conversely, upon cycling, at the end of a complete cycle, the plastic strains in the bond coat cause the stress in the TGO to decrease below its yield strength. The consequence is an ability to introduce additional growth strain at the temperature maximum, with associated elongation of the TGO (Fig. 9). This repeats on a cycle-by-cycle basis enabling cyclic enlargement. The details depend on the yield strengths for the TGO and bond coat and the growth strain per cycle.

3.3. The basic model

The basic model is derived for a thin TGO, relative to the sphere radius, such that gradients in the TGO are negligible. However, it has only been possible to derive analytic solutions in the absence of reverse yielding on reheating (Appendix A), fomenting the following strategy. Analytic formulae provide non-dimensional groupings that facilitate understanding and correlate the overall trend. Specific results are obtained numerically, covering a broad range of parameter space (relative to the full geometric model).

When the bond coat responds elastically, the increments of TGO stress and displacement are given by [21]:

$$\Delta\sigma_{tgo} = -\frac{\Delta\varepsilon_T E_{tgo}}{\left[\frac{3E_{tgo}h}{2E_{bc}R} + (1 - \nu_{tgo})\right]} \equiv -\Delta\varepsilon_T \Lambda E_{tgo}, \quad (2a)$$

$$\Delta u = \frac{3\Delta\varepsilon_T E_{tgo} \Lambda h}{2E_{bc}} \quad (2b)$$

with

$$\Lambda = \left[\frac{3E_{tgo}h}{2E_{bc}R} + (1 - \nu_{tgo})\right]^{-1}$$

The corresponding change in the radial stress at the interface is:

$$\begin{aligned} \Delta\sigma_{rr} &\equiv \frac{2\Delta\sigma_{tgo}h}{R} \\ &= -2\Lambda E_{tgo} \Delta\varepsilon_T h/R \end{aligned} \quad (2c)$$

The tangential stresses are:

$$\Delta\sigma_{\theta\theta} = \Delta\sigma_{\phi\phi} = -(1/2)\Delta\sigma_{rr}.$$

The transformation strain increment, $\Delta\varepsilon_T$, requires some explanation. While the TGO is elastic, $\Delta\varepsilon_T$ is either the thermal expansion misfit, $-\Delta\alpha\Delta T$, or the growth strain, $\Delta\varepsilon_g$, depending on the segment of the thermal history (cooling/reheating or growth, respectively). When the TGO reaches yield, internal growth exerts no pressure change: requiring that $\Delta\varepsilon_T = 0$ during that part of the growth segment.

When a portion of the bond coat reaches yield, the non-linear equation relating the plastic zone size R_p to the accumulated transformation strain, ε_T , is:

$$\frac{1}{2} \left(\frac{R_p}{R}\right)^3 + \frac{(1 - \nu_{tgo})E_{bc}R}{E_{tgo}h} \left(\frac{1}{3} + \ln\left(\frac{R_p}{R}\right)\right) = \frac{\varepsilon_T}{\varepsilon_Y^{bc}} \quad (3)$$

where $\varepsilon_Y^{bc} = \sigma_Y^{bc}/E_{bc}$. The stresses and plastic displacements are:

$$\frac{\sigma_{tgo}}{\sigma_Y^{bc}} = -\frac{R}{h} \left[\frac{1}{3} + \ln\left(\frac{R_p}{R}\right)\right] \quad (4a)$$

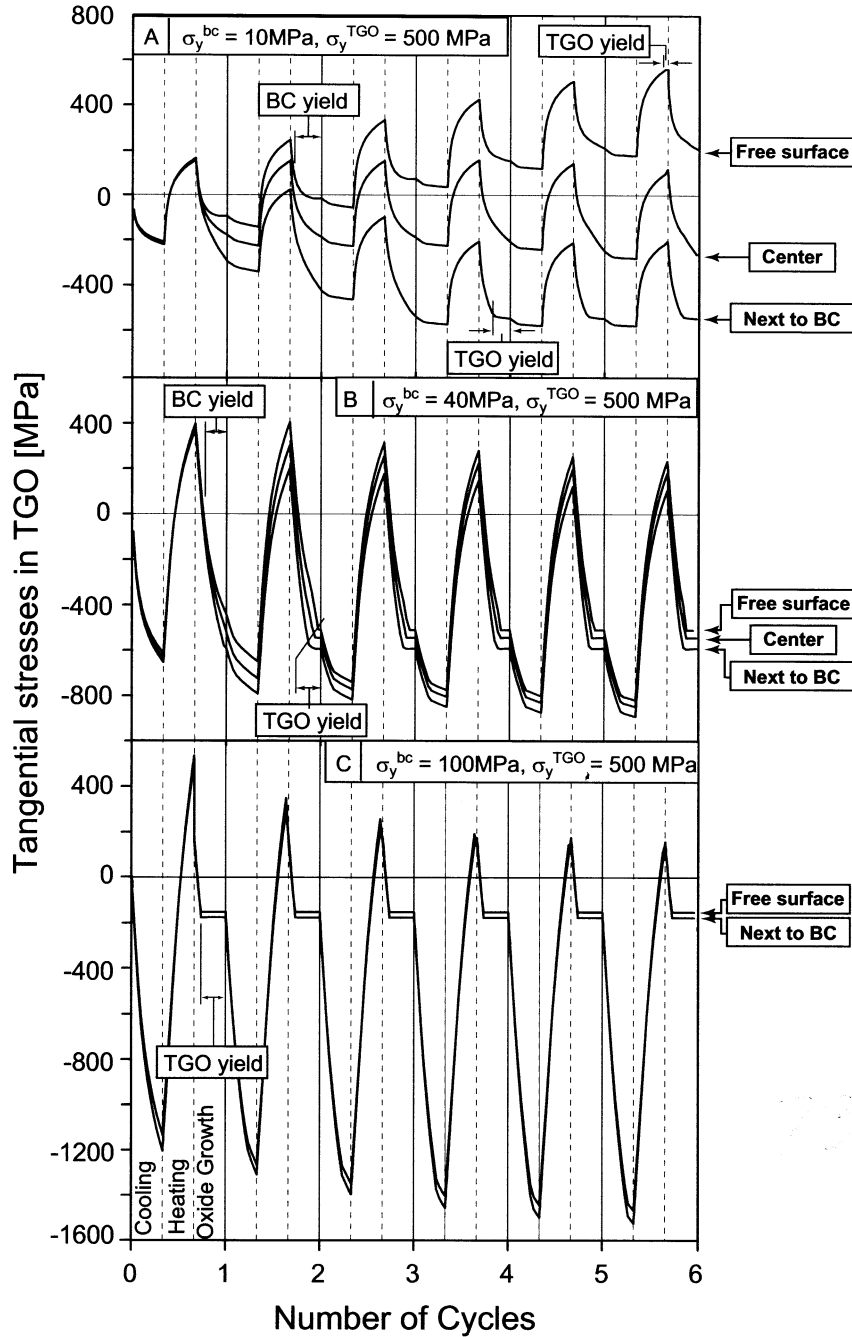


Fig. 13. The development of tangential stresses in the TGO over the first thermal cycles for (A) $\sigma_Y^{bc} = 10$ MPa, (B) $\sigma_Y^{bc} = 40$ MPa, (C) $\sigma_Y^{bc} = 100$ MPa show a stress gradient over the TGO for the lower bond coat yield strength, resulting in TGO yielding in tension upon reheating. For the higher yield strength, the TGO yields during growth strain, in compression. (D) The radial enlargement for $\sigma_Y^{bc} = 10, 20$ and 40 MPa is limited by the TGO yielding.

$$\frac{u_{pl}}{R} = \frac{\epsilon_Y^{bc}}{2} \left(\frac{R_p}{R} \right)^3 \quad (4b)$$

The radial and tangential stresses in the bond coat are related through the yield condition:

$$|\sigma_{\theta\theta} - \sigma_{rr}| = \sigma_Y^{bc}$$

Note that in Eq. (3), ϵ_T is the sum of all increments in

$-\Delta\alpha\Delta T$ and $\Delta\epsilon_g$ when the TGO is not at yield. One limit is of interest.

When the yield strain for the bond coat is small and tends to zero ($\epsilon_Y^{bc} \rightarrow 0$), Eqs. (3) and (4b) give the maximum possible displacement per cycle:

$$\frac{u_{max}}{R} \rightarrow \epsilon_T \quad (4c)$$

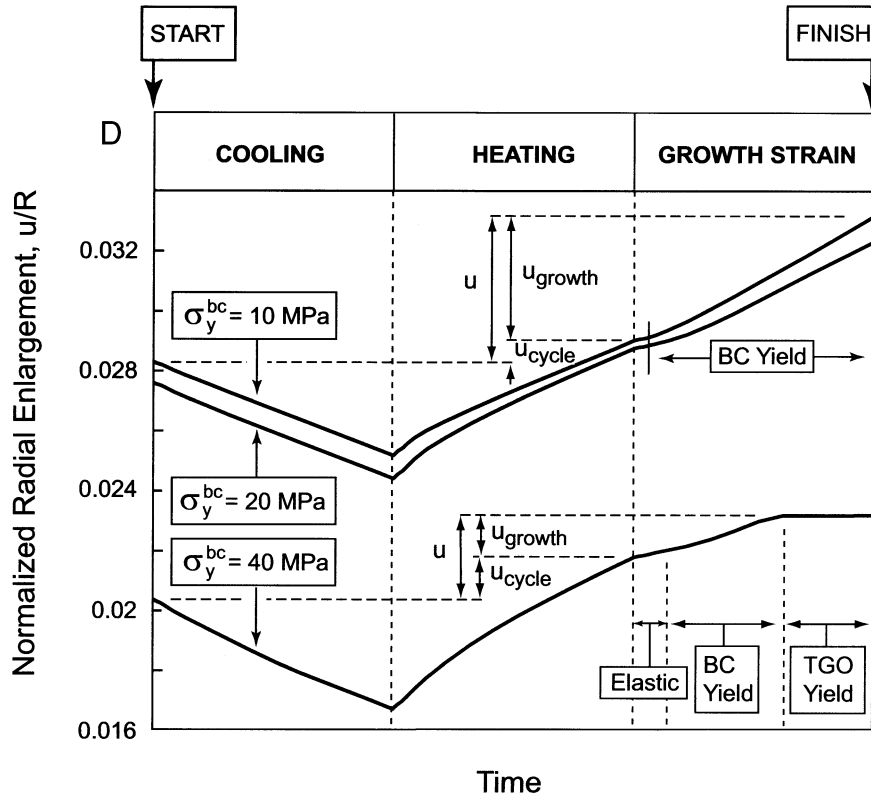


Fig. 13 (Continued)

That is, as the back-pressure from the bond coat reduces toward zero, all of the potential TGO displacement provided by the growth strain is enabled.

3.4. Finite thickness effects

When the bond coat is relatively soft and h/R is finite, stress gradients develop in the TGO. The gradient arises because the addition of a tangential growth strain within a spherical shell results in incompatibility, requiring a radially-variable elastic strain to accommodate the misfit. The difference in tangential stress between the TGO surface, σ_{tgo}^s , and the interface, σ_{tgo}^I , is given by:

$$\sigma_{\text{tgo}}^s - \sigma_{\text{tgo}}^I = -\frac{E_{\text{tgo}} \Delta \varepsilon_g}{(1 - \nu_{\text{tgo}})} \ln \left(1 + \frac{h}{R} \right) + \sigma_{rr} \quad (5a)$$

When the bond coat is at yield, the first term in Eq. (5a) exceeds the second, such that the largest stress difference arises as $\sigma_Y^{\text{bc}} \rightarrow 0$, with the stress at the surface, σ_{tgo}^s , being more tensile than at the interface, σ_{tgo}^I .

In practice, at high temperature, such large stress gradients cannot be sustained. Instead, the associated gradient in chemical potential results in a mass counter-flux by grain boundary diffusion, tending to eliminate the gradient. A simple scaling argument based on the through-thickness chemical potential gradient caused by the stresses normal to the columnar grain boundaries and the diffusive flux along them indicates that the

maximum allowable stress difference is

$$[\sigma_{\text{tgo}}^s - \sigma_{\text{tgo}}^I]_{\text{max}} = -\frac{\Delta \varepsilon_g}{t_{\text{hot}}} \left[\frac{h^2 D k T}{D_b \delta_b \Omega} \right] \quad (5b)$$

where D is the TGO grain size (Fig. 6), k is the Boltzmann constant, Ω is the molecular volume and $D_b \delta_b$ is the grain boundary diffusivity. Inserting values for bulk alumina at 1400 K [37] indicates that the stress differences of only about 10 MPa can be sustained. In practice, the effect of cations incorporated into the TGO may decrease the diffusivity relative to bulk alumina [29–31], enabling higher levels of stress difference.

3.5. Simulations

For simulation purposes, the TGO yield strength is equated to the growth stress (-100 MPa to -1 GPa), while the bond coat yield strength, $(\sigma_Y^{\text{bc}})_{\text{min}}$, is considered to be in the range measured on Pt–aluminide materials at strain-rates representative of those expected upon thermal cycling (5–100 MPa, see Fig. 10), in the temperature range $\Delta T \equiv T_{\text{max}} - T_2$. The calculations presented here focus on two issues. (a) The influence of the bond coat strength and of the TGO growth stress on the displacement per cycle. (b) The role of the time that the configuration is held at the peak temperature during each cycle, t_{hot} . An assessment of the stresses in the TGO and of the radial enlargement, based on the

typical results shown on Fig. 13 (Appendix B), motivates the ensuing summary.

(i) The influence of material properties is summarized on Fig. 14, which plots the cumulative displacement after 24 cycles as a function of bond coat strength for several levels of growth stress. The displacement per cycle increases as the bond coat becomes softer and as the TGO growth stress increases. Note that, for typical TGO growth stresses, the displacement attains the maximum possible value, u_{\max}/R (Eq. (4c)), when $\sigma_Y^{bc} < 20$ MPa. This maximum changes as the number of cycles increases. At the low strength levels, a large stress gradient develops in the TGO (Fig. 13B), as expected from Eqs. (5a) and (5b). This causes the tensile stress induced near the TGO surface to reach yield on reheating (Appendix B). Conversely, the stress induced during growth causes it to yield in compression near the interface. While these behaviors are complex, they do not appear to be important since the displacements still attain the maximum allowed by the growth process (Fig. 14; Eq. (4c)).

(ii) A hot time effect arises provided that the TGO reaches yield during the growth step. At large t_{hot} , the TGO is at yield for most of the time, such that the growth strain results in thickening with minimal elongation (Fig. 9). Conversely, upon cycling, at the end of a complete cycle, the plastic strains in the bond coat cause the stress in the TGO to decrease below yield. The consequence is an ability to introduce additional growth strain during the next cycle [21]. The cumulative radial enlargement as the system cycles, obtained for different t_{hot} (Fig. 15), represents the basic input. In the figure, the shortest hold time is designated, $t_{\text{hot}} = t_0$. It coincides with a growth strain, $\Delta\epsilon_g = 5 \times 10^{-4}$. Other values of t_{hot} are multiples of t_0 (up to $20t_0$ or $\Delta\epsilon_g = 10^{-2}$). A fit to the results indicates that the displacement per cycle, du/dN , varies with hold time as:

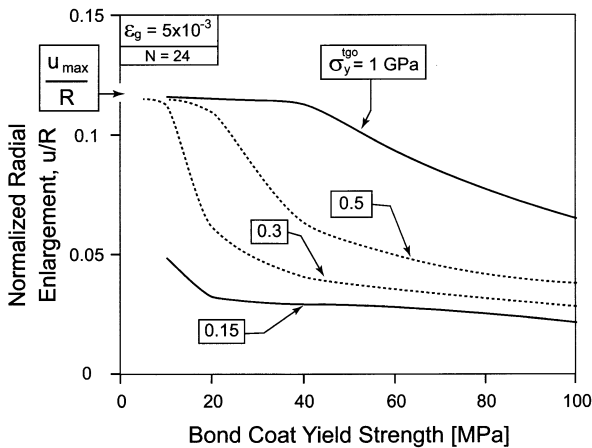


Fig. 14. Trends in radial enlargement after 24 cycles predicted by the sphere model. Note that the limit displacement is reached for soft bond coats, in agreement with Eq. (4c).

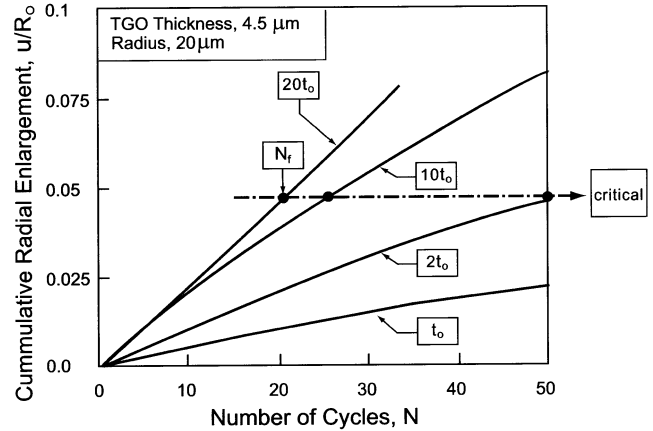


Fig. 15. The development of the radial enlargement for various choices of the hot time (time at temperature).

$$\frac{du/dN}{R} \approx 5 \times 10^{-4} \left(\frac{t_{\text{hot}}}{t_0} \right)^{1/2} \quad (6)$$

where t_0 is a reference time. In turn, for parabolic oxidation kinetics, the hold time is related to the TGO thickness by [6]:

$$h = \sqrt{2kNt_{\text{hot}}} \quad (7)$$

where k is the parabolic rate constant. Should the life be governed by a specified TGO displacement, u_c , a combination of Eqs. (6) and (7) would predict a critical TGO thickness at failure:

$$h_c \approx 70(ku_c/R)^{1/2}(t_{\text{hot}}t_0)^{1/4} \quad (8)$$

This trend is consistent with experimental findings that compare the durability between furnace cycle and burner rig configurations [42]. Namely, for the burner rig configuration, subject to smaller t_{hot} , the TGO at failure is much thinner.

4. Layered systems

The preceding sphere model is not capable of addressing layer effects (Fig. 5A). Two such effects are considered to be particularly important. (a) The cracking of the TBC above the TGO instabilities and the interaction of the cracks with the instability (Fig. 3). (b) The plastic response of the bond coat when the misfit due to either thermal contraction or phase transformations is sufficient to elicit a fully plastic response upon thermal cycling.

When intact, the thermal barrier layer has sufficient stiffness to inhibit downward displacement of the TGO, but it experiences normal tensile stresses (Fig. 16) [20]. Given the existence of weak deposition planes in the TBC [15,17,43], this stress is sufficient to create cracks, which locally eliminate the constraint of the TBC, allowing the instability to propagate at a rate essentially

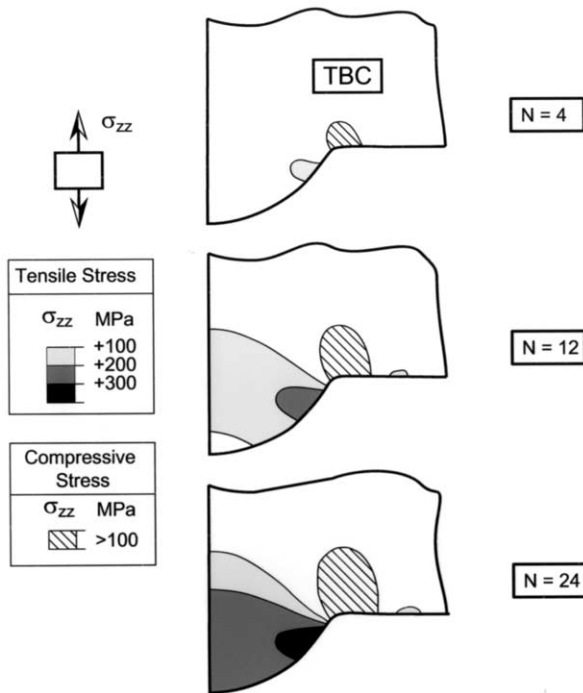


Fig. 16. A synopsis of the evolution of out-of plane stresses in the TBC over 24 thermal cycles.

the same as that absent in the TBC (Fig. 3). This localization of the instability differentiates it from the response when the top layer is absent.

Once cracks have been induced, the TGO displacement is able to proceed, locally. This causes the TGO to ‘push-up’ on the TBC, resulting in cycle-by-cycle extension of the cracks (Fig. 17). A full crack growth simulation protocol, coupled with the TGO instability, is needed to address these effects [44].

In typical thermal barrier systems, there is a substantial strain misfit on cooling between the bond coat and the substrate, caused by thermal contraction and phase transformations. This misfit is often sufficient to cause the bond coat to become fully plastic upon thermal cycling. When this happens, the TGO is susceptible to the development of instabilities with well-defined wavelength. The amplitude of these instabilities depends on the initial imperfection size and increases on a cycle-by-cycle basis to an extent critically dependent on the misfit strain. Analysis of this type is in progress [45].

5. Summary

A simulation protocol for TGO displacements found in a class of thermal barrier systems has been described. It has been shown to be consistent with observations whenever the bond coat and TGO are both capable of yielding. The TGO must yield at the peak temperature,

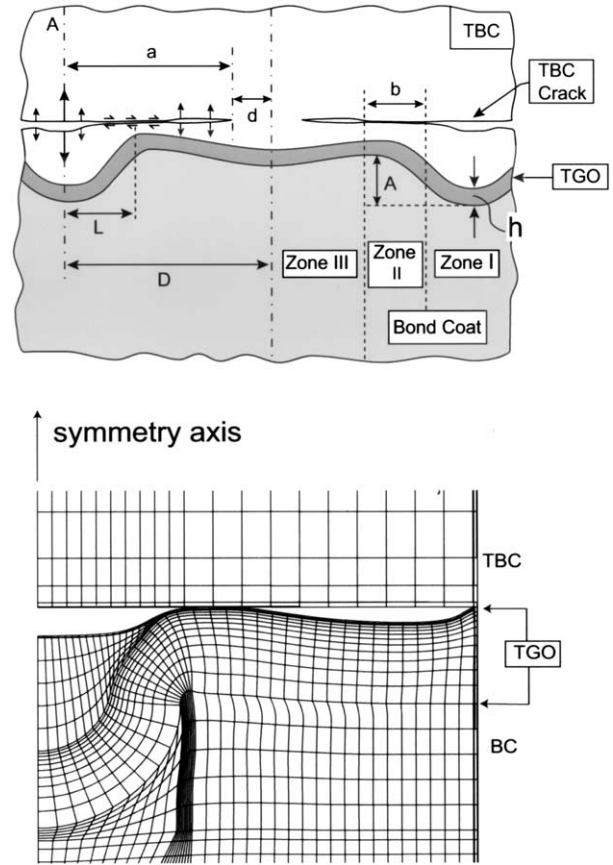


Fig. 17. Schematic of cracks in the TBC above the TGO imperfections and a finite element simulation showing the TGO ‘pushing-up’ the TBC at the perimeter of the imperfection [42].

during growth. The bond coat must yield on cooling. Reverse yielding of the bond coat upon heating is not required, but when it occurs, it exacerbates the displacement. The displacement rate increases as the yield strength of the bond coat is reduced, because of the greater plastic accommodation of the growth strain. An upper limit is reached when the bond coat is sufficiently soft, $\sigma_Y^{bc} < 20$ MPa. Accordingly, bond coats most susceptible to this instability are those with compositions in the β -phase field, because of the relatively inferior high temperature strength of this phase.

An intact TBC layer suppresses the TGO instability. However, the stresses in the TBC are sufficiently large that cracks are induced. In turn, these cracks allow the displacements to proceed, locally, with ensuing coupling between the extent of cracking in the TBC and the TGO displacement.

Plastic/creep deformation of the TGO is needed to account for the effects of hold time, t_{hot} . Decreasing the TGO strength reduces the displacement rate. The magnitude of the elongation strain relative to the thickening of the TGO does not appear to be critical, provided that the TGO is able to yield. This insensitivity arises because, once yielding commences, the stress is

not able to increase, whereupon the pressure imposed on the bond coat remains constant and there is no further displacement. The additional strain is redistributed as thickening. Results obtained using a sphere model have been used to rationalize the influence of the hold time. At long t_{hot} , the TGO remains at yield for a larger fraction of the cumulative hot time. During this time, there is no TGO elongation and minimal cyclic displacement. It is also apparent that those TGO compositions and microstructures with the largest growth stress are most susceptible to the instability.

Appendix A: Analysis using the sphere model

The complete cycle consists of the six segments outlined in Fig. 12. The cycle commences [1] with stresses, $(\sigma_{\text{tgo}})_1$, $(\sigma_{rr})_1$, $(\sigma_{\theta\theta})_1$. Imposing a growth strain, $\Delta\varepsilon_{\text{g}}$, results in stresses at segment [2] given by:

$$\begin{aligned}(\sigma_{\text{tgo}})_2 &= (\sigma_{\text{tgo}})_1 - \Delta\varepsilon_{\text{g}}^* E_{\text{tgo}} \Lambda \\ (\sigma_{rr})_2 &= (\sigma_{rr})_1 - 2\Delta\varepsilon_{\text{g}}^* E_{\text{tgo}} \Lambda h/R \\ (\sigma_{\theta\theta})_2 &= (\sigma_{\theta\theta})_1 + \Delta\varepsilon_{\text{g}}^* E_{\text{tgo}} \Lambda h/R\end{aligned}\quad (\text{A1})$$

where $\Delta\varepsilon_{\text{g}}^* = \Delta\varepsilon_{\text{g}}$ when $(\sigma_{\text{tgo}})_2 < \sigma_{\text{Y}}^{\text{tgo}}$; but otherwise,

$$\Delta\varepsilon_{\text{g}}^* = (1/\Lambda E_{\text{tgo}})[\sigma_{\text{Y}}^{\text{tgo}} - (\sigma_{\text{tgo}})_1] \quad (\text{A2})$$

with

$$\Lambda = \left[\frac{3E_{\text{tgo}}h}{2E_{\text{bc}}R} + (1 - \nu_{\text{tgo}}) \right]^{-1}$$

On cooling, when the bond coat yields at segment [3], the stresses are:

$$\begin{aligned}(\sigma_{\text{tgo}})_3 &= (\sigma_{\text{tgo}})_1 - \Delta\varepsilon_{\text{g}}^*(R/h)E_{\text{tgo}}\Lambda h/R \\ &\quad - \Delta\alpha[\Delta T - \Delta T_{\text{pl}}]\Lambda E_{\text{tgo}} \\ (\sigma_{rr})_3 &= (\sigma_{rr})_1 - 2\Delta\varepsilon_{\text{g}}^* E_{\text{tgo}} \Lambda h/R \\ &\quad - 2\Delta\alpha[\Delta T - \Delta T_{\text{pl}}]\Lambda E_{\text{tgo}} h/R \\ (\sigma_{\theta\theta})_3 &= (\sigma_{\theta\theta})_1 + \Delta\varepsilon_{\text{g}}^* E_{\text{tgo}} \Lambda h/R \\ &\quad + \Delta\alpha[\Delta T - \Delta T_{\text{pl}}]\Lambda E_{\text{tgo}} h/R\end{aligned}\quad (\text{A3})$$

$$|(\sigma_{\theta\theta})_3 - (\sigma_{rr})_3| = \sigma_{\text{Y}}^{\text{bc}}$$

Moreover, as demonstrated by the simulations, reverse yielding occurs on reheating such that the initial values of the radial and tangential stresses are also related by the yield condition for the bond coat. Hence, except for the first cycle:

$$\Delta T_{\text{pl}} = \Delta T - \left[\frac{2\sigma_{\text{Y}}^{\text{bc}} - 3\Delta\varepsilon_{\text{g}}^* \Lambda E_{\text{tgo}} h/R}{3\Delta\alpha \Lambda E_{\text{tgo}} h/R} \right] \quad (\text{A4a})$$

In the first cycle:

$$\Delta T_{\text{pl}} = \Delta T - \left[\frac{\sigma_{\text{Y}}^{\text{bc}} - 3\Delta\varepsilon_{\text{g}}^* \Lambda E_{\text{tgo}} h/R}{3\Delta\alpha \Lambda E_{\text{tgo}} h/R} \right] \quad (\text{A4b})$$

Once yielding has occurred, the stresses may be obtained from Eqs. (4c), (4b) and (4c) provided that there has been no reverse yielding. To progress, since the simulations reveal that the radial stresses in the bond coat (as well as the stresses in the TGO) increase with imperceptible non-linearity upon reheating, reverse yielding is neglected. The errors incurred are revealed upon comparing the analytic results with full simulations. It has been found that the errors accumulate after the first 10 cycles with appreciable discrepancies arising after 50 cycles. This deficiency limits the utility of the analytic results.

Absent prior reverse yielding, the stresses at step [4] are:

$$\begin{aligned}(\sigma_{\text{tgo}})_4 &= -\sigma_{\text{Y}}^{\text{bc}} \frac{R}{h} \left[\frac{1}{3} + \ln \frac{(R_{\text{p}})_4}{R} \right] \\ (\sigma_{rr})_4 &= \frac{2h}{R} (\sigma_{\text{tgo}})_4 \\ |(\sigma_{\theta\theta})_4 - (\sigma_{rr})_4| &= \sigma_{\text{Y}}^{\text{bc}}\end{aligned}\quad (\text{A5})$$

with the plastic zone size given by the implicit relation:

$$\begin{aligned}\frac{1}{2} \left(\frac{(R_{\text{p}})_4}{R} \right)^3 + \frac{(1 - \nu_{\text{tgo}}) E_{\text{bc}}}{E_{\text{tgo}}} \frac{R}{h} \left[\frac{1}{3} + \ln \frac{(R_{\text{p}})_4}{R} \right] \\ = \frac{\Sigma(\Delta\varepsilon_{\text{g}}^* + \Delta\alpha\Delta T)}{\varepsilon_{\text{Y}}^{\text{bc}}}\end{aligned}\quad (\text{A6})$$

On reheating, again because the simulations demonstrate linearity in the radial stress (as if the bond coat were elastic), the stresses at step [6] become:

$$\begin{aligned}(\sigma_{\text{tgo}})_6 &= (\sigma_{\text{tgo}})_4 + \Delta\alpha\Delta T E_{\text{tgo}} \Lambda \\ (\sigma_{rr})_6 &= (\sigma_{rr})_4 + 2\Delta\alpha\Delta T E_{\text{tgo}} \Lambda h/R \\ |(\sigma_{\theta\theta})_6 - (\sigma_{rr})_6| &= \sigma_{\text{Y}}^{\text{bc}}\end{aligned}\quad (\text{A7})$$

The stresses at [6] become those at the start of the next cycle [1], $(\sigma_{\text{tgo}})_1$, $(\sigma_{rr})_1$, $(\sigma_{\theta\theta})_1$. The process then repeats.

The permanent displacement associated with these stresses is then determined from Eq. (3a) with the growth strain obtained from Eq. (A2), and the plastic zone size from Eq. (A6). After each cycle, the radius and TGO thickness are updated in accordance with:

$$\begin{aligned}R_6 &= R_1 + \Delta u_{\text{growth}} + \Delta u_{\text{cycle}} \\ h_6 &\equiv h_2 = h_1 + k\sqrt{t_{\text{hot}}}\end{aligned}\quad (\text{A8})$$

where t_{hot} is the time spent at the temperature maximum and k is the parabolic rate constant for TGO thickening.

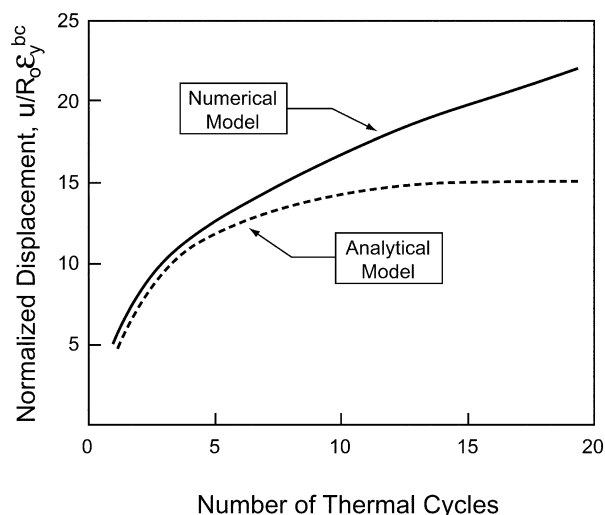


Fig. A1. The accumulation of the radial enlargement during 20 thermal cycles using results from the numerical and the analytical model. The models agree for only the first five cycles.

A comparison between analytic results and those obtained numerically (Fig. A1) indicates the discrepancies that arise after about 10 cycles.

Appendix B: Assessment of the stresses in the TGO and the displacements per cycle

The tangential stress in the TGO over the first six thermal cycles, determined for three levels of bond coat yield strength, for $\sigma_{Y}^{tgo} = 500$ MPa, has been summarized on Fig. 13(A–C). Each cycle consists of cooling–heating–oxide growth steps, as indicated. Stresses at three radial locations are shown: (i) in an element next to the bond coat, (ii) in an element in the center of the TGO, and (iii) in an element next to the free surface. For high bond coat yield strength, $\sigma_{Y}^{bc} = 100$ MPa, Fig. 13C, the stresses are uniform, with negligible gradient. During oxide growth, the TGO yields in compression (throughout its thickness), while the bond coat remains elastic. This is consistent with the thin shell analytical model presented in the text. This scenario changes at lower bond coat yield strength (Fig. 13A and B). Now the bond coat yields during oxide growth, and the TGO experiences a stress gradient, such that its yielding response is no longer uniform. The stress gradient develops during oxide growth, as discussed in the text (Eq. (5a)) and increases with each cycle. The effect is most vivid at the lowest bond coat yield strength, $\sigma_{Y}^{bc} = 20$ MPa, as anticipated by (Eq. (5a)), even resulting in large tensile stresses at the inner surface. In consequence, after about five thermal cycles, the inner surface of the TGO yields in tension during the final stage of reheating. Comparison between the stress gradient found in the simulations, at each yield strength, with

the analytic result (Eq. (5a)) indicates agreement within 15%.

While lower bond coat yield strength generally increases the radial enlargement (Fig. 14), the effect diminishes at the lowest yield strengths (Fig. 13D) as the upper bound (Eq. (4c)) is approached. This is apparent upon comparing the displacements during a single cycle when $\sigma_{Y}^{bc} = 10$ and 20 MPa. For the softer bond coats, most of the displacement occurs during oxide growth, u_{growth} , because growth can be accommodated by the bond coat without yielding the TGO. Conversely, for the stronger bond coats, ($\sigma_{Y}^{bc} = 40$ MPa in Fig. 13D), u_{growth} is smaller, because the TGO yields during the growth step, and the displacement develops predominantly during cooling and reheating, u_{cycle} .

References

- [1] R.A. Miller, J. Am. Ceram. Soc. 67 (1984) 517.
- [2] T.E. Strangman, Thin Solid Films 127 (1985) 93.
- [3] P.K. Wright, A.G. Evans, Current Opinion Solid State Mater. Sci. 4 (1999) 255.
- [4] M.J. Stiger, N.M. Yanar, M.G. Topping, F.S. Pettit, G.H. Meier, Z. für Metallkunde 90 (1999) 1069.
- [5] J.T. DeMasi-Marcin, D.K. Gupta, Sur. Coatings Technol. 68/69 (1994) 1.
- [6] A.G. Evans, D.R. Mumm, J.W. Hutchinson, G.H. Meier, F.S. Pettit, Prog. Mater. Sci. 46 (2001) 505.
- [7] N.P. Padture, M. Gell, E.H. Jordan, Science 296 (2002) 280.
- [8] C.A. Johnson, J.A. Ruud, R. Bruce, D. Wortman, Surf. Coat. Technol. 109 (1998) 80.
- [9] M. Gell, K. Vaidyanathan, B. Barber, J. Cheng, E. Jordan, Metall. Mater. Trans. 30A (1999) 427.
- [10] V. Tolpygo, D.R. Clarke, Acta Materialia 48 (2000) 3283.
- [11] D.R. Mumm, A.G. Evans, Acta Materialia 48 (2000) 1815.
- [12] M.Y. He, A.G. Evans, J.W. Hutchinson, Acta Materialia 48 (2000) 2593.
- [13] J.M. Ambrico, M.R. Begley, E.H. Jordan, Acta Materialia 49 (2001) 1577.
- [14] A.M. Karlsson, A.G. Evans, Acta Materialia 49 (2001) 1793.
- [15] D.R. Mumm, A.G. Evans, I. Spitsberg, Acta Materialia 49 (2001) 2329.
- [16] D.R. Mumm, A.G. Evans, Key Eng. Mater. 197 (2001) 199.
- [17] J.A. Ruud, A. Bartz, M.P. Borom, C.A. Johnson, J. Am. Ceram. Soc. 84 (2001) 1545.
- [18] M.Y. He, J.W. Hutchinson, A.G. Evans, Acta Materialia 50 (2002) 1063.
- [19] A.M. Karlsson, C.G. Levi, A.G. Evans, Acta Materialia 50 (2002) 1263.
- [20] A.M. Karlsson, T. Xu, A.G. Evans, Acta Materialia 50 (2002) 1211.
- [21] A.M. Karlsson, W.J. Hutchinson, A.G. Evans, J. Mech. Phys. Solids 50 (2002) 1565.
- [22] I. Spitsberg, D.R. Mumm, A.G. Evans, J. Mater. Res., in press.
- [23] B. Gleeson, W. Wang, D.J. Sordelet, Iowa State University, unpublished research, 2002.
- [24] K.L. Johnson, J. Mech. Phys. Solids 18 (1970) 115.
- [25] K.L. Johnson, Contact Mechanics, Cambridge University Press, Cambridge UK, 1985.
- [26] R. Hill, B. Storåkers, A.B. Sdunek, Proc. R. Soc. Lond. A 423 (1989) 301.

- [27] A.G. Evans, M.Y. He, J.W. Hutchinson, *Acta Materialia* 45 (1997) 3543.
- [28] R.M. Cannon, W.H. Rhodes, A.H. Heuer, *J. Am. Ceram. Soc.* 63 (1980) 46.
- [29] J. Cho, M.P. Harmer, H.M. Chan, J.M. Rickman, A.M. Thompson, *J. Am. Ceram. Soc.* 80 (1997) 1013.
- [30] J. Fang, A.M. Thomson, M.P. Harmer, H.M. Chan, *J. Am. Ceram. Soc.* 80 (1997) 2005.
- [31] R.M. Cannon, P.Y. Hou, High temperature corrosion and materials chemistry, *Electrochem. Soc. Proc.* 98/99 (1998) 594.
- [32] A.G. Evans, R.M. Cannon, *Mater. Sci. Forum* 43 (1989) 243.
- [33] A.G. Evans, M.Y. He, J.W. Hutchinson, *Prog. Mtls Sci.* 46 (2001) 249.
- [34] V.K. Tolpygo, J.R. Dryden, D.R. Clarke, *Acta Materialia* 46 (1998) 927.
- [35] N. Rebello, M.Y. He, C.G. Levi, A.G. Evans, *Z. Metallkund*, in press.
- [36] D.R. Clarke, *Acta Materialia*, in press.
- [37] H.J. Frost, M.F. Ashby, *Deformation mechanism maps*, Pergamon Press, New York, 1982.
- [38] D. Pan, M.W. Chen, P.K. Wright, K.J. Hemker, *Acta Materialia*, submitted for publication.
- [39] M.W. Chen, R.T. Ott, T.C. Hufnagel, P.K. Wright, K.J. Hemker, *Surface Coatings Technology*, in press.
- [40] M.R. Begley, A.G. Evans, J.W. Hutchinson, *Int. J. Solids Struc.* 36 (1999) 2773.
- [41] M.R. Begley, D.R. Mumm, A.G. Evans, J.W. Hutchinson, *Acta Materialia* 48 (2000) 3211.
- [42] D.R. Mumm, M. Watanabe, A.M. Karlsson, A.G. Evans, J. Pfaendtner, *Acta Materialia*, submitted for publication.
- [43] S.G. Terry, C.G. Levi, *Materials Science and Engineering*, submitted for publication.
- [44] T. Xu, M.Y. He, A.G. Evans, *Interface Science*, submitted for publication.
- [45] D. Balint, J.W. Hutchinson, in press.